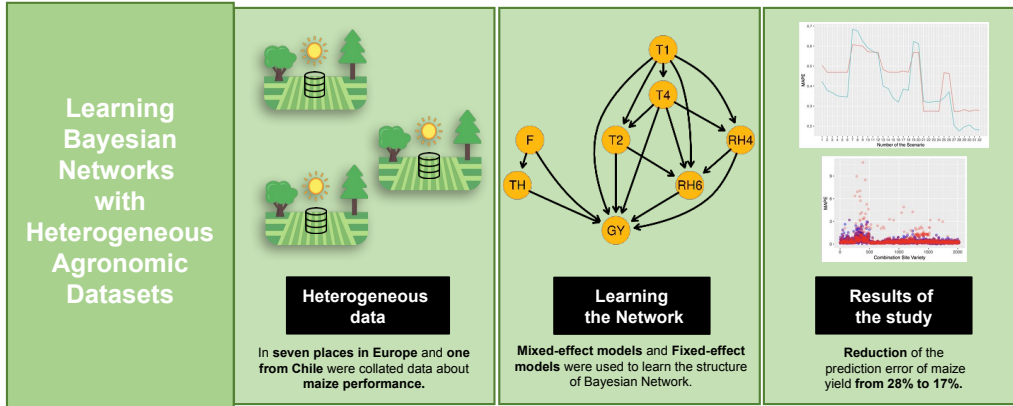


arXiv:2308.06399v1
Graphical Abstract

Learning Bayesian Networks with Heterogeneous Agronomic Data Sets via Mixed-Effect Models and Hierarchical Clustering

Lorenzo Valleggi, Marco Scutari, Federico Mattia Stefanini



Highlights

Learning Bayesian Networks with Heterogeneous Agronomic Data Sets via Mixed-Effect Models and Hierarchical Clustering

Lorenzo Valleggi, Marco Scutari, Federico Mattia Stefanini

- Using mixed-effects models in the learning procedure leads to discovering new arcs.
- Clustering improves the learning procedure.
- Prediction error of the BN maize grain yield decreases approximately from 28% to 17%.

Learning Bayesian Networks with Heterogeneous Agronomic Data Sets via Mixed-Effect Models and Hierarchical Clustering

Lorenzo Valleggi^a, Marco Scutari^b, Federico Mattia Stefanini^c

^a*Department of Statistics, Computer Science and Applications, University of Florence, Florence, Italy*

^b*Istituto Dalle Molle di Studi sull'Intelligenza Artificiale (IDSIA), Lugano, Switzerland*

^c*Department of Environmental Science and Policy, University of Milan, Milan, Italy*

Abstract

Maize is a major crop providing vital calories in sub-Saharan Africa, Asia and Latin America, with a global cultivation area of 197 million hectares in 2021. Therefore, many statistical models (such as mixed-effect and random coefficients models) and machine learning models (such as random forests and deep learning architectures) have been developed to predict maize yield and how it is affected by genotype, environment and genotype-environment interaction factors, including field management. However, these models do not fully leverage the network of causal relationships between these factors and the hierarchical structure of the agronomic data arising from data collection.

Bayesian networks (BNs) provide a powerful framework for modelling causal and probabilistic relationships using directed acyclic graphs to illustrate the connections between variables. This study introduces a novel approach that integrates random effects into BN learning. Rooted in the linear mixed-effects models framework, it is particularly well-suited to hierarchical data. Results from a real-world agronomic trial suggest that the proposed approach enhances BN learning, leading to a more interpretable model and discovering new causal connections. At the same time, the error rate of maize yield prediction is reduced from 28% to 17%. Therefore, we argue that BNs should be the tool of choice to construct practical decision support tools for hierarchical agronomic data that allow for causal inference.

Keywords: hierarchical data sets, Bayesian networks, causal networks,

1. Introduction

The global economy relies on agriculture as a vital source of income and employment as well as food, ensuring food quality and safety, environmental preservation, fostering comprehensive rural development, and upholding social cohesion in rural areas. Given the projected global population growth, which is expected to reach 9.7 billion by 2050 (Pew Research Center, 2019), it is estimated that global agricultural production must increase by 60% (Alexandratos and Bruinsma, 2012) to meet the increase in demand. With these premises, improving crop management systems is becoming essential to match future needs. Maize is one of the most widely cultivated crops in sub-Saharan Africa, Asia and Latin America, with a total area of 197 M ha (FAO et al., 2021). It provides almost all the caloric intake in the Americas (285 kcal/capita/day) and in Africa (374 kcal/capita/day; FAO-STAT, 2019). Predicting the grain yield of this cultivar provides valuable information about the expected crop output before harvest, enabling more effective management practices. To achieve accurate predictions, it is essential to consider the interplay between genotype, environment, and field management. Widely adopted statistical models for this task include linear mixed-effect and random coefficient models that use genome-wide association study (GWAS) to study the causal effects of genotype, environmental variables and their interactions (Zorić et al., 2022; Ndlovu et al., 2022; Tolley et al., 2023; Rotili et al., 2020).

More recently, machine learning models such as random forests (Yang et al., 2022; Leroux et al., 2019), naive Bayes and SVM (Mupangwa et al., 2020) have been applied to maize crop yield prediction using multi-temporal UAV remote sensing data. Deep learning architectures such as Long Short-Term Memory (LSTM; Zhang et al., 2021; Krishna et al., 2023) and Convolutional Neural Network (CNN; Yang et al., 2021) have also been explored. Despite their predictive performance, which rests on their ability to encode complex non-linear relationships, these models are not causal in nature. Outside of randomised experiments, they are particularly vulnerable to confounding (Pearl, 2009), that is, learning spurious associations as causal relationships due to unobserved variables acting as common causes of treatment and outcome and or due to selection bias. They also often disregard

the hierarchical structure that is typical of the data collected in agronomic studies, which is highly informative.

In general, studies encompassing heterogeneous collections of related data sets (RDs) in which the relationships between the covariates and the outcome of interest may differ (say, in slope or variance; Gelman and Hill, 2007) are widespread in many fields, from clinical trials to environmental science (Spiegelhalter et al., 2004; Qian et al., 2010). Hierarchical (multilevel) models are commonly adopted to pool information across different subsets of the data while accounting for their specific features (Gelman et al., 2014). However, heterogeneity is not the only challenge in fitting a model on such data: the variables involved are typically related by a complex network of causal relationships, making their joint distribution is challenging to learn (especially) from small data sets.

In this work, we chose to learn a Bayesian Network (BN) from RDs focused on the agronomic performance of maize. BNs can be learned and used as *causal network models* whose arcs represent cause-effect relationships and which can be used for causal inference following the work of Judea Pearl (Pearl, 2009). In the case of RDs, learning BNs is also related to *transfer learning* (Pan and Yang, 2010), which is not widely documented in the literature. Transfer learning has mainly focused on applications involving deep learning, with very few publications involving BNs. Notably, recent work by Yan et al. (2023) proposed a structure learning approach based on conditional independence tests for operational adjustments in a flotation process characterised by a small data set with a limited sample size. To induce transfer learning, they considered the results of the independence tests performed on variables X_i and X_j in both the source and target data sets, which differed in terms of sample size. Other authors have suggested the use of order-search algorithms to learn BN structures, introducing a structural bias term to facilitate the transfer of information between data sets and achieve more robust networks (Oyen and Lane, 2015). BNs and structural equation models have proven successful in the agronomic sector, optimising various management practices such as phytosanitary treatments (Lu et al., 2020), irrigation management strategies (Ilić et al., 2022) and soil management (Hill et al., 2017), to minimise environmental impact and mitigate climate change. However, in the agronomic literature, transfer learning has predominantly focused on crop disease classification using deep learning techniques like convolutional neural networks (Coulibaly et al., 2019; Paymode and Malode, 2022), with little research involving BNs.

We learned the structure and the parameters of a Conditional Gaussian Bayesian Network (CGBN) from a real-world agronomic data set that has a hierarchical structure. In order to account for the high heterogeneity that characterises such data, we developed a novel approach that integrates random effects into the local distributions in the BN, building on Scutari et al. (2022). Random effects are the salient feature of *linear mixed-effects models* (LME; Pinheiro and Bates, 2000). LME models are hierarchical models that extend the classical linear regression model by adding a second set of coefficients, called “random effects”, which are jointly distributed as a multivariate normal. The other coefficients are called “fixed effects”. The coefficients associated with the random effects have mean zero, and they naturally represent the deviations of the effects of the parents in individual data sets from their average effects across data sets, which is represented by the fixed effects.

The hierarchical estimation in BNs learned from RDs was originally introduced by Azzimonti et al. (2019), who proposed a novel approach to tackle this challenge for discrete BNs using a hierarchical multinomial-Dirichlet model. That approach outperforms a traditional multinomial-Dirichlet model and is competitive with random forests, but as the number of domains increases, the estimation becomes more complex, necessitating the use of approximations such as variational or Markov chain Monte Carlo inference.

The remainder of the paper is structured as follows. In Section 2, we briefly describe the data set (Section 2.1), we introduce the background of BN (Section 2.2), we introduce the local distributions and the structure learning approach used to learn the BN (Section 2.3) and we how we evaluated its performance (Section 2.4). In Section 3, we present and evaluate the BN, and in Section 4, we discuss its performance before suggesting possible future research directions.

2. Materials and Methods

2.1. Background of Bayesian network

Bayesian networks (BNs; Koller and Friedman, 2009) provide a powerful tool to learn and model highly structured relationships between variables. A BN is a graphical model defined on a set of random variables $\mathbf{X} = \{X_1, \dots, X_K\}$ and a directed acyclic graph (DAG) \mathcal{G} that describes their relationships: nodes correspond to random variables and the absence of arcs between them implies the conditional independence or the lack of direct causal effects (Pearl, 2009). In particular, a variable X_i is independent of all

other non-parent variables in \mathcal{G} given the set of variables associated with its parents $pa(X_i)$. A DAG \mathcal{G} then induces the following factorisation:

$$P(\mathbf{X} \mid \mathcal{G}, \Theta) = \prod_{i=1}^K P(X_i \mid pa(X_i), \Theta_{X_i}), \quad (1)$$

where Θ_{X_i} are the parameters of the conditional distribution of $X_i \mid pa(X_i)$. In equation (1), the *joint multivariate distribution* of \mathbf{X} is reduced to a collection of univariate conditional probability distributions, the *local distributions* of the individual nodes X_i . If all sets $pa(X_i)$ are small, (1) is very effective in replacing the high-dimensional estimation of Θ with a collection of low-dimensional estimation problems for the individual Θ_{X_i} . Another consequence of (1) is the existence of the *Markov blanket* of each node X_i , the set of nodes that makes X_i conditionally independent from the rest of the BN. It comprises the parents, the children and the spouses of X_i , and includes all the knowledge needed to do inference on X_i , from estimation to hypothesis testing to prediction.

The process of learning a BN from data can be divided into two steps:

$$\underbrace{P(\mathcal{G}, \Theta \mid \mathcal{D})}_{\text{BN learning}} = \underbrace{P(\mathcal{G} \mid \mathcal{D})}_{\text{structure learning}} \cdot \underbrace{P(\Theta \mid \mathcal{G}, \mathcal{D})}_{\text{parameter learning}}.$$

Structure learning aims to find the dependence structure represented by the DAG given the data \mathcal{D} . Several algorithms are described in the literature for this task. Constraint-based algorithms such as the PC algorithm (Spirtes et al., 2000) use a sequence of independence tests with increasingly large conditioning sets to find which pairs of variables should be connected by an arc (or not), and then they identify arc directions based on the difference in conditional independence patterns between v-structures (of the form $X_j \rightarrow X_i \leftarrow X_k$, with no arc between X_j and X_k) and other patterns of arcs. Score-based algorithms instead use heuristics (like hill climbing; Russell and Norvig, 2009) or exact methods (as in Cussens, 2012) to optimise a network score that reflects the goodness of fit of candidate DAGs to select an optimal one. *Parameter learning* provides an estimate of Θ through the parameters in the Θ_{X_i} conditional to the learned DAG.

Structure learning algorithms are distribution-agnostic, but the choice of the conditional independence tests and of the network scores depends on the types of distributions we assume for the X_i . The three most common choices

are *discrete BNs*, in which the X_i are multinomial random variables; *Gaussian BNs* (GBNs), in which the X_i are univariate normal random variables linked by linear dependence relationships; and *conditional Gaussian BNs* (CGBNs), in the X_i are either multinomial random variables (if discrete) or mixtures of normal random variables (if continuous). Common scores for all these choices are the Bayesian information criterion (BIC; Schwarz, 1978) or the marginal likelihood of \mathcal{G} given \mathcal{D} (Heckerman and Geiger, 1995). As for the conditional independence tests, we refer the reader to Edwards (2000), which covers various options for all types of BNs.

Parameter learning uses maximum-likelihood estimates or Bayesian posterior estimates with non-informative priors for all types of BNs (Koller and Friedman, 2009). All the conditional independence tests, the network scores and the parameter estimators in the literature referenced above can be computed efficiently thanks to (1) because they factorise following the local distributions.

2.2. The Data Set: Agronomic Performance of Maize

This study uses the data from Millet et al. (2019), whose authors are well-known in plant science research. They conducted a *randomised* genome-wide association study to assess the genetic variability of plant performance under different year-to-year and site-to-site climatic conditions. The original analysis of these data in (Millet et al., 2016) confirms the quality of this experimental design in terms of controlling both confounding and various sources of noise. Overall, 29 field experiments were arranged in Europe, nine sites, and in Chile, one site: each of them was defined by a combination of year, site and water regime (watered or rain-fed), and 244 *varieties* of maize (*Zea mays L.*) were studied. Each experiment was designed as alpha-lattice design (Patterson and Williams, 1976), with two replicates of the watered regime and three for the rain-fed regime. The data were collected at experimental sites in France, Germany, Italy, Hungary, Romania, and Chile between 2011 and 2013. After filtering out incomplete observations, the study analysed eight *sites*, each with different sample size: Gaillac (France, $n = 2437$), Nerac (France, $n = 1716$), Karlsruhe (Germany, $n = 2626$), Campagnola (Italy, $n = 1260$), Debrecen (Hungary, $n = 2181$), Martonvasar (Hungary, $n = 1260$), Craiova (Romania, $n = 1055$), and Graneris (Chile, $n = 760$). Many weather variables were measured for each site, such as air temperature, relative humidity (RH), wind speed and light; they were measured every hour at 2m height. Soil water potential was measured daily at

30, 60, and 90cm depths. For this analysis, we decided to use only air temperature and RH because they are the more basic variables that can describe plant growth. Since weather variables were measured for each site instead of for each plot, we decided to aggregate the weather data in order to have the *average temperature* ($^{\circ}C$), the *diurnal temperature range*, the *average relative humidity* (%) and the *diurnal relative humidity range* (%) for each site and year for three different periods, which correspond to the main phenological stages of maize: seeding, germination, and emergence of the seeds, the vegetative phase where leaves emerge (May to June), the flower development, pollen shedding, grain development (July to August), maturation of the grain and harvest (September to October). Furthermore, random noise with a mean of 0 and a standard deviation of 0.1 was added to each weather observation to simulate the sensor’s measurement error and avoid blocks of identical measurements in each individual site.

At the end of the experiment, the phenological variables listed below were measured for each plot at each site:

- The *grain yield* adjusted at 15% grain moisture, in ton per hectare (t/ha).
- The *grain weight* of individual grains (mg).
- The *anthesis*, male flowering (pollen shed), in thermal time cumulated since emergence ($d20^{\circ}C$).
- The *sinking*, female flowering (silking emergence), in thermal time cumulated since emergence ($d20^{\circ}C$).
- The *plant height* from ground level to the base of the flag leaf (highest leaf (cm)).
- The *tassel height*, plant height including tassel, from ground level to the highest point of the tassel (cm).
- The *ear height*, ear insertion height, from ground level to the ligule of the highest ear leaf (cm).

2.3. Learning Algorithm

We learned the structure of the BN, denoted \mathcal{B}_{LME} , following the steps in Algorithm 1.

Algorithm 1: Structure learning \mathcal{B}_{LME} .

Data: data set \mathcal{D} , *blacklist*, and a *whitelist*

Result: The DAG \mathcal{G}_{max} that maximises $\text{BIC}(\mathcal{G}_{max}, \mathcal{D})$.

1. Run a linear regression on grain yield and extract the residuals ϵ_i .
 2. For each Site \times Variety combination, compute the mean and the standard deviation of ϵ_i .
 3. Perform hierarchical clustering on the means and standard deviations of the residuals from each site-variety combination.
 4. Add a new variable with the cluster labels to \mathcal{D} .
 5. Compute the score of \mathcal{G} , $\mathcal{S}_{\mathcal{G}} = \text{BIC}(\mathcal{G}, \mathcal{D})$ and set $\mathcal{S}_{max} = \mathcal{S}_{\mathcal{G}}$ and $\mathcal{G}_{max} = \mathcal{G}$.
 6. *Hill-climbing*: repeat as long as \mathcal{S}_{max} increase:
 - (a) Add, delete or reverse all possible arc in \mathcal{G}_{max} resulting in a DAG.
 - i. compute BIC of the modified DAG \mathcal{G}^* , $\mathcal{S}_{\mathcal{G}^*} = \text{BIC}(\mathcal{G}^*, \mathcal{D})$;
 - ii. if $\mathcal{S}_{\mathcal{G}^*} > \mathcal{S}_{max}$ and $\mathcal{S}_{\mathcal{G}^*} > \mathcal{S}$ set $\mathcal{G} = \mathcal{G}^*$ and $\mathcal{S}_{\mathcal{G}} = \mathcal{S}_{\mathcal{G}^*}$.
 - (b) Update \mathcal{S}_{max} with the new value of $\mathcal{S}_{\mathcal{G}^*}$.
 7. Return the DAG \mathcal{G} .
-

For the hill-climbing algorithm, we used the implementation in the *bnlearn* R package (Scutari, 2010) and the BIC score. We provided a list of arcs to be excluded (*blacklist*) or included (*whitelist*) by hill-climbing to avoid evaluating unrealistic relationships (such as Average temperature of July-Aug \rightarrow Average temperature of May-June).

Firstly, we regressed the grain yield against all the available variables for all combinations of site and variety. We used the mean and the variance of the residuals from the regression for each combination of site and variety to cluster them using the agglomerative Ward clustering algorithm (Murtagh and Legendre, 2014) from the *stats* R package. The resulting discrete variable was added to the data used to identify the RDs.

Following the approach and the notation described in Scutari et al. (2022), we assumed that each RD is generated by a GBN, and that all GBNs share a common underlying network structure but different parameter values. In order to ensure the partial pooling of information between RDs, the clusters are made a common parent for all phenological variables and incorporated in

the local distributions as a random effect. Therefore, we modelled the local distributions for those variables as a linear mixed-effect model using the *lme4* R package (Bates et al., 2015):

$$\begin{aligned}
X_{i,j} &= (\mu_{i,j} + b_{i,j,0}) + \mathbf{\Pi}_{X_i}(\beta_i + b_{i,j}) + \epsilon_{i,j}, \\
\begin{pmatrix} b_{i,j,0} \\ b_{i,j} \end{pmatrix} &\sim N(\mathbf{0}, \tilde{\Sigma}_i), \\
(\epsilon_{i,1}, \dots, \epsilon_{i,j}, \dots)^T &\sim N(\mathbf{0}, \sigma_i^2 \mathbf{I}_{n_j})
\end{aligned} \tag{2}$$

where bold letters indicate matrices. The only exception was grain yield because it also required a model for variances which have been implemented using *nlme* R package (Heisterkamp et al., 2017) as follows:

$$\begin{aligned}
X_{i,j} &= (\mu_{i,j} + b_{i,j,0}) + \mathbf{\Pi}_{X_i} \beta_i + \epsilon_{i,j}, \\
b_{i,j,0} &\sim N(0, \sigma_{b,i}^2), \\
&N(0, (\sigma_{i,1}^2, \sigma_{i,2}^2, \dots, \sigma_{i,j}^2, \dots) \mathbf{I}_{n_j}), \\
(\epsilon_{i,1}, \dots, \epsilon_{i,j}, \dots)^T &\sim N(\mathbf{0}, (\sigma_{i,1}^2, \dots, \sigma_{i,j}^2, \dots) \mathbf{I}_{n_j}), \\
\sigma_{i,j}^2(\nu) &= |\nu|^{2\theta_j}.
\end{aligned} \tag{3}$$

In both (2) and (3), the notation is as follows:

- $j = 1, \dots, J$ are the clusters identifying the RDs;
- $\mathbf{\Pi}_{X_i}$ is the design matrix associated to the parents of X_i ;
- $b_{i,j,0}$ is the random intercept;
- $b_{i,j}$ is the random slope parameter for the j th cluster;
- $\tilde{\Sigma}_i$ is the $n_j \times n_j$ block of Σ_i associated with the j th cluster;
- $\sigma_{i,j}^2 \mathbf{I}_{n_j}$ is the $n_j \times n_j$ matrix arising from the assumption that residuals are homoscedastic in (2);
- $\mu_{i,j}$ is the intercept;
- and β_i are the fixed effects.

In (3), we assumed the variance of residuals to be heteroscedastic and following a power function, where ν is the variance covariate and θ_j is the variance function coefficient that changes for every level of the common discrete parent.

We modelled the weather variables using only fixed effects for simplicity:

$$X_i = \mu_i + \mathbf{\Pi}_{X_i}\beta_i + \epsilon_i, \quad \epsilon_i \sim N(0, \sigma_i^2 \mathbf{I}_n). \quad (4)$$

We prevented the clusters from being their parent with the blacklist because the resulting arcs are not of interest from an agronomic perspective.

From these assumptions, the BN \mathcal{B}_{LME} we learned from the data has a global distribution that is a mixture of multivariate normal distributions like a CGBN.

2.4. Predictive and Imputation Accuracy

The most important variable in this analysis was grain yield because it is one of the key quantities used to evaluate an agronomic season. To assess the predictive ability of \mathcal{B}_{LME} , we evaluated the Mean Absolute Percentage Error (MAPE) of:

- the *predictive accuracy* of grain yield predictions in the scenarios listed in Table A.1, which are meant to study the potential effect of measuring a reduced set of variables in future years;
- the *imputation accuracy* for the grain yield in each site-variety combination, which we removed in turn and imputed from the rest.

As a term of comparison, we used a CGBN learned from the data (\mathcal{B}_{CGBN}) and compared its performance with that of \mathcal{B}_{LME} . We implemented both prediction and imputation using likelihood weighting (Koller and Friedman, 2009; Darwiche, 2009).

To validate the learning strategy in Algorithm 1, we performed 50 replications of hold-out cross-validation where 20% of the site-variety combinations were sampled and set aside to be used as a test set. The remaining 80% was used as a training set to learn \mathcal{B}_{LME} and \mathcal{B}_{CGBN} . We computed the predictions for each phenological node X_i (except for grain yield) from its Markov blanket and used these predictions to predict the grain yield in turn. We used the kernel densities of the predicted values and the resulting credible intervals with coverage 0.80 to assess the amount of variability in prediction.

We are aware that predictive accuracy is not an adequate measure of performance for a causal model, which is why we also validated it using expert knowledge from the literature in Section 4. However, it allows for comparisons with other machine learning models which cannot be assessed causally, and it can be used to evaluate specific loss functions for \mathcal{B}_{LME} in different application settings.

3. Results

The complete BNs \mathcal{B}_{LME} and \mathcal{B}_{CGBN} learned from the data are shown in the Supplemental Material; here, we show only the subgraph around the variable grain yield for each BN in Figure 1 and 2. Following Section 2.3, we identified 60 site-variety clusters (with only 5 containing fewer than 100 observations) and used them as a discrete variable set to be the parent of the phenological nodes.

The structure of \mathcal{B}_{LME} is more complex than that of \mathcal{B}_{CGBN} : \mathcal{B}_{LME} has 118 arcs compared to the 92 of \mathcal{B}_{CGBN} , and the average Markov blanket size reflects that (17 for \mathcal{B}_{LME} , 12 for \mathcal{B}_{CGBN}). Notably, we discovered more relationships for the phenological nodes, particularly for the grain yield variable (Table A.2), which had eight more parents than in \mathcal{B}_{CGBN} .

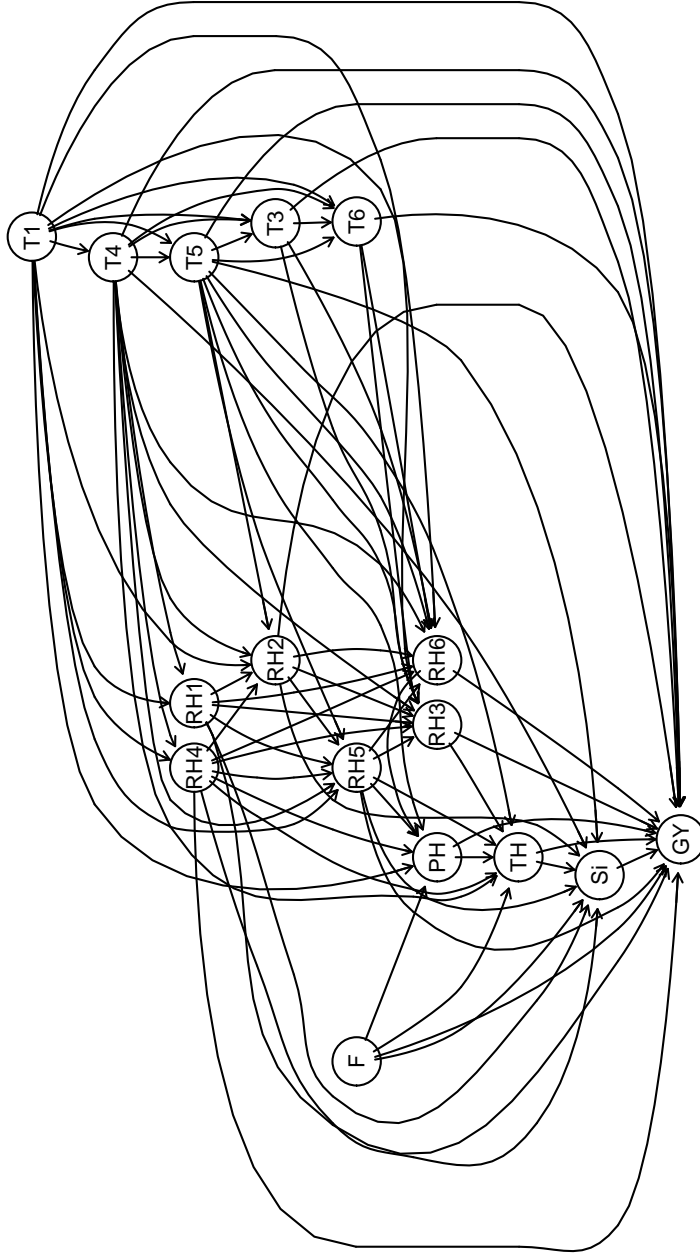


Figure 1: Structure of the BN \mathcal{B}_{LME} learned with Algorithm 1. The nodes represent: the average temperature May-June (T1), the average temperature Sept-Oct (T3), the diurnal temperature range May-June (T4), the diurnal temperature range July-Aug (T5), the diurnal temperature range Sept-Oct (T6), the average RH May-June (RH1), the average RH July-Aug (RH2), the average RH Sept-Oct (RH3), the diurnal RH range May-June (RH4), the diurnal RH range July-Aug (RH5), the diurnal RH range Sept-Oct (RH6), Silking (Si), TH (Tassel height), PH (Plant height), EH (Ear height) and F (Clusters).

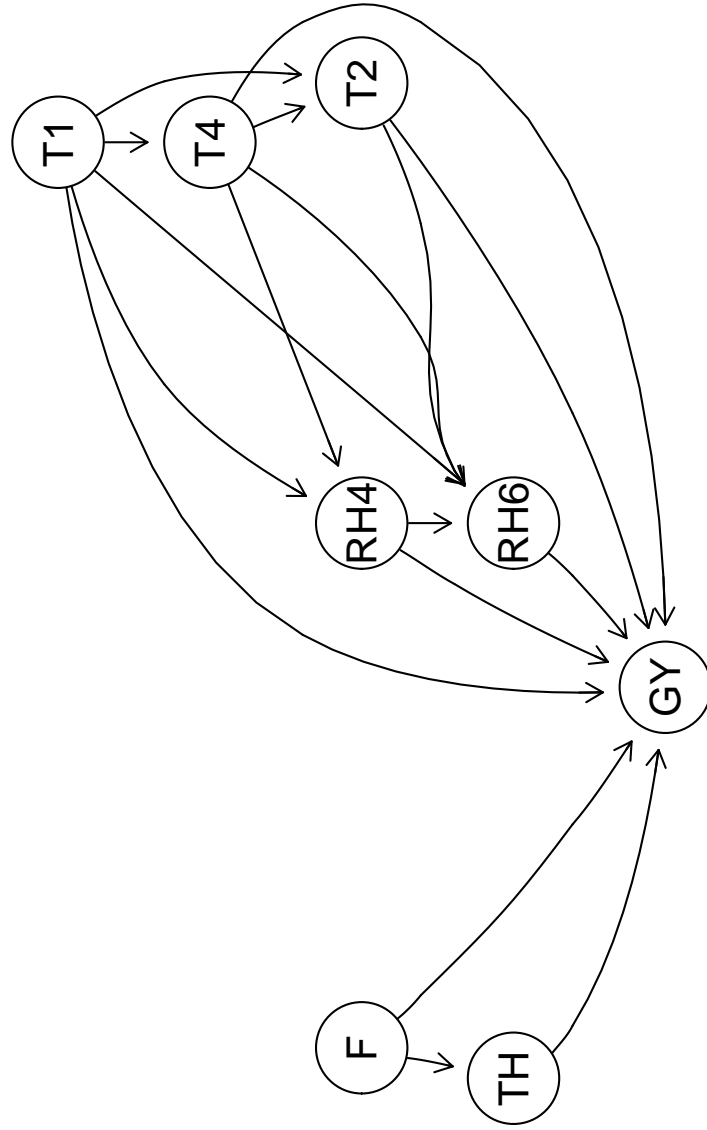


Figure 2: Structure of the BN \mathcal{B}_{CGBN} . The nodes represent: the average temperature May-June (T1), the average temperature July-Aug (T2), the diurnal temperature range May-June (T4), the diurnal RH range May-June (RH4), the diurnal RH range Sept-Oct (RH6), TH (Tassel height) and F (Clusters).

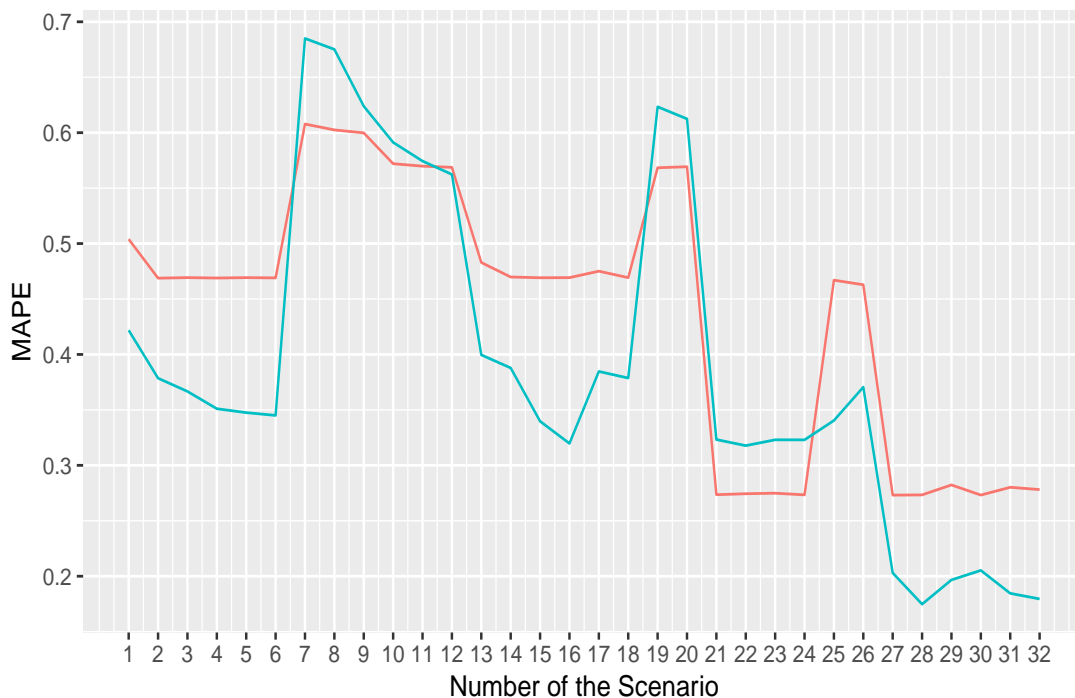


Figure 3: Prediction accuracy of the learned BNs, \mathcal{B}_{LME} (blue line) and \mathcal{B}_{CGBN} (orange line), in terms of grain yield Mean Absolute Percentage Error (MAPE) of each scenario of evidence propagation (definitions of the scenarios are reported in Table A.1). Lower values are better.

The predictive accuracy for each of the scenarios reported in Table A.1 is shown in Figure 3 for both \mathcal{B}_{LME} and \mathcal{B}_{CGBN} . Overall, \mathcal{B}_{LME} outperformed \mathcal{B}_{CGBN} in terms of MAPE. The exception was in a few cases, specifically scenarios 7 to 11, 19, 20 and from 21 to 24, where \mathcal{B}_{CGBN} demonstrated a lower MAPE than \mathcal{B}_{LME} , albeit with a difference in MAPE of only 0.06. In contrast, when \mathcal{B}_{LME} outperformed \mathcal{B}_{CGBN} , the difference in MAPE was 0.14. This trend was particularly evident in scenarios 27 to 32, where an increasing usage of weather/phenological variables was provided. As expected, the scenarios with the lowest MAPE were those that utilised the Markov Blanket (scenario 31) and the parents of grain yield (scenario 32).

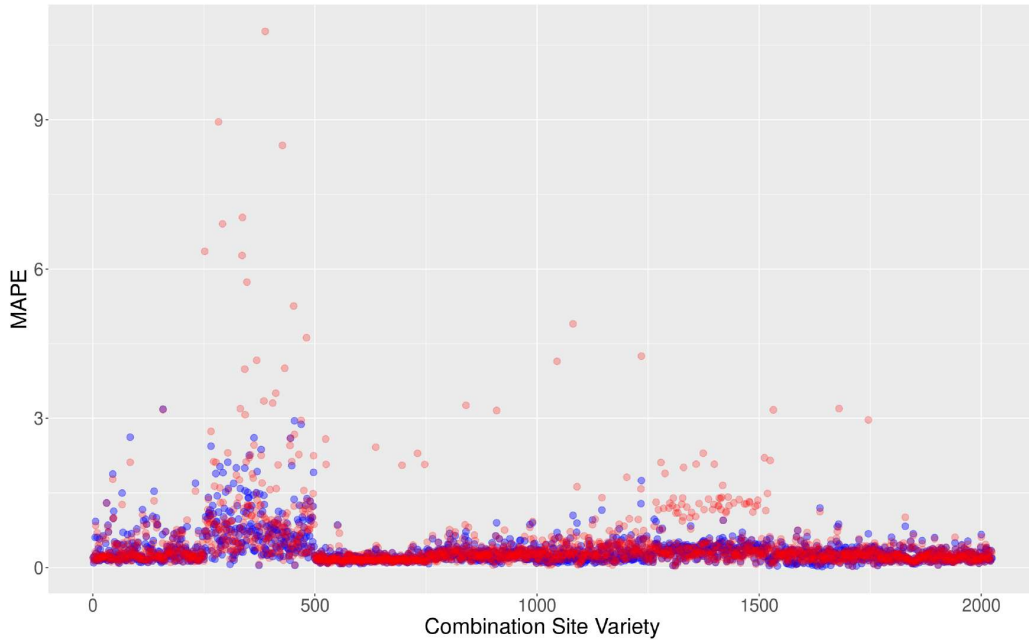


Figure 4: Imputation accuracy of the learned BNs, \mathcal{B}_{LME} (blue points) and \mathcal{B}_{CGBN} (red points), in terms of grain yield Mean Absolute Percentage Error (MAPE) of each site-variety combination, shown sequentially for brevity. Lower values are better.

The MAPE for the imputation of different site-variety combinations is shown in Figure 4. We observe that \mathcal{B}_{LME} and \mathcal{B}_{CGBN} perform similarly for all combinations except those involving the sites of Craiova (numbered 250–500) and Campagnola (numbered 1250–1500), for which \mathcal{B}_{CGBN} has a higher MAPE than \mathcal{B}_{LME} .

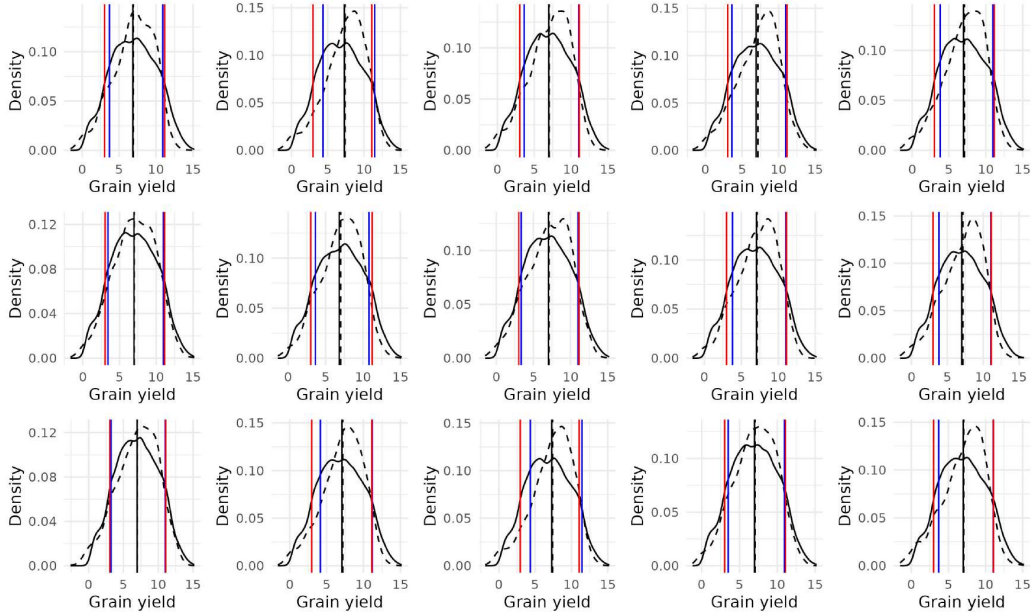


Figure 5: Kernel densities of the grain yield in the training set are represented by the solid curve, while the dashed curve depicts the kernel densities of the predicted grain yield obtained through likelihood-weighted approximation during cross-validation. The kernel density-based credible interval at 80% for the grain yield in the training set is indicated by the red line and for the predicted grain yield by the blue line. The mean is reported with a solid line for the grain yield of the training set and a dashed line for the predicted grain yield.

The kernel densities of grain yield for the first 15 runs of cross-validation are shown in Figure 5. The densities for the training set exhibit somewhat heavier tails compared to those for the predicted values. Furthermore, the predictive densities have narrower credible intervals compared to those from the training set, particularly on the lower tail, and are more often positively skewed. The mean values are nearly identical for both, at approximately $7t/ha$, with a 0.8 credible interval $[4t/ha, 11t/ha]$.

Finally, we employed a step-wise parent elimination algorithm to search for non-significant effects in each of the local distributions of the phenological variables. The BIC values consistently indicated that, within \mathcal{B}_{LME} , the best set of effects were those selected by our method. The only exception was the

variable “tassel height,” for which the BIC was lower when the “diurnal RH range July-August” variable was omitted. The same procedure was applied with the removal of random effects from the local distributions. In this case, the set of effects selected by our method still yielded the best BIC values. Furthermore, we conducted a comparison of the BIC values for local distributions with and without the random effects. Generally, the presence of random effects improved goodness of fit, except for the variables “tassel height” and “silking,” which exhibited better BIC values in the absence of random effects. All BIC results are reported in Table A.3 and Table A.4. The BIC values of the first row correspond to the set of parents of the local distribution found with our method, and the other rows correspond to the BIC value found after each parent elimination.

4. Discussion

In this paper, we used a Bayesian network (BN) to analyse the results of a multi-site agronomic experiment comprising eight different sites in Europe and Chile. Our goal was to obtain a network model that can be used for causal inference, thus providing an ideal foundation to develop decision support systems to manage maize crops. In order to do that effectively, we modified the structure learning of the BN to encode the hierarchical structure of the data, thus addressing the violation of the exchangeability assumption that characterises the RDs.

The data we used consisted of weather variables and phenological variables of maize measured from 2011 to 2013. In our study, we selected a subset of variables based on their agronomic relevance in addition to the weather variables for temperature and humidity. The latter was measured daily for each site, so we calculated their mean for specific time-slices corresponding to the key phenological phases of maize, namely seeding, germination, emergence (May-June); vegetation stage, tasselling, silking, ear formation (July-August); and grain filling, maturation and harvest (September-October). The reason for this choice was to capture the effect of each weather variable on the phenological variables. Based on strong prior knowledge, specific arcs were prohibited due to their lack of causal meaning. For example, it is not plausible for a weather variable from a later time slice to affect another in an earlier time slice. We applied the same logical reasoning to the connections between phenological variables that are recorded in different time slices: for instance, the arc from grain yield to silking was prohibited, as it

is causally impossible for the grain yield to cause female flowering (silking). Moreover, all arcs that made the cluster variable a child of other variables were prohibited.

We compared the structures of the BN incorporating random effects (\mathcal{B}_{LME}) to the baseline including only fixed effects (\mathcal{B}_{CGBN}): the former contains 26 additional arcs compared to the latter, with a significant difference in the case of grain yield which had 8 more parents. We further assessed the predictive accuracy of phenological variables in both \mathcal{B}_{LME} and \mathcal{B}_{CGBN} using the Diebold-Mariano test (Diebold and Mariano, 2002). This statistical evaluation allowed us to determine that the predictive accuracy improvement observed in \mathcal{B}_{LME} was statistically significant for all of the variables (p-value < 0.05 , results not shown). We are aware that predictive accuracy is not an adequate measure of performance for a causal model, which is better assessed using expert knowledge as we do below, but it provides a term of comparison for our model in the wider context of machine learning models, which cannot be assessed causally.

Regarding grain yield, plant height emerged as a new parent: its role as a reliable predictor for maize grain yield is well-documented in the literature (Yin et al., 2011; Pugh et al., 2018). Additionally, its ease of measurement using remote sensing makes it a suitable candidate for predicting maize grain yield (Han et al., 2018; Chu et al., 2018). Supporting evidence comes from the work of Anderson et al. (2019), who studied 280 hybrids conducted in 1,500 plots using unmanned aerial systems and found a positive correlation between plant height and maize grain yield. Another new parent identified in the analysis is silking. This finding is also supported by existing evidence, as Malik et al. (2005) demonstrated a significant negative correlation between silking and grain yield. They posited that this negative relationship could be attributed to late female flowering, resulting in a less favourable photoperiod and low temperature induced by changing seasons. Considering variables related to temperature and relative humidity (RH), they are all the parents of grain yield in \mathcal{B}_{LME} but not in \mathcal{B}_{CGBN} , where only diurnal RH range May-June (RH4), diurnal RH range Sept-Oct (RH6), average temperature May-June (T1), average temperature July-Aug (T2), diurnal temperature range May-June (T4) were present. This is plausible since environmental conditions are very important for maize growth: for instance, evidence shows that high humidity during flowering promotes the maize yield (Butts-Wilmsmeyer et al., 2019). Temperature plays a crucial role in influencing maize yield, particularly during the reproductive phase, where sub-optimal

or supra-optimal values can have a significant impact. For instance, temperatures ranging from 33°C to 36°C during the pre-and post-flowering stages can result in a reduction of grain yield by 10% to 45% (Neiff et al., 2016). In a review by Waqas et al. (2021), the detrimental effects of thermal stress on maize growth were thoroughly examined from both an agronomic and a physiological perspective. They emphasised that high temperatures, especially during the flowering period, can have various adverse consequences on floret number, silk number, and grain development. Furthermore, the process of fertilisation and grain-filling may also be compromised under such conditions. On the other hand, low temperatures below 10°C can also be detrimental, negatively impacting the normal growth process of maize. Such cold temperatures can limit germination, adversely affect root morphology, and decrease the efficiency of photosystem II. These combined factors demonstrate the sensitivity of maize to temperature fluctuations, which can significantly influence its growth and overall productivity.

We applied hierarchical clustering to the mean and the variance of the residuals from a simple linear regression of the grain yield, which was selected due to its agronomic relevance, against all other variables to avoid making any assumptions about the possible parent grain yield. After grouping the residuals by site-variety combination, hierarchical clustering produced 60 relatively-balanced clusters: they were included in the data as a discrete variable that was set as a common parent of the phenological variables in a setup similar to a conditional Gaussian BN as described in Section 2.3. We decided to use the clusters, rather than just the site of origin or the maize variety as individual variables, for two reasons:

- When using either the site or the maize variety as a common discrete parent variable, we found the dispersion of residuals in the local distribution, particularly that of grain yield, to be non-homogeneous.
- Combining the site of origin and the maize variety without clustering their combinations produces a variable with approximately 1200 possible values, which would make BN structure learning computationally prohibitive.

As a result, we improved both the computational feasibility and the predictive accuracy of the model. Using clustering as a pre-processing step has been proposed in the literature to find suitable scenarios in risk assessment analysis (Pettet et al., 2017) or to reduce the dimension of the estimation

problem, learning the structure of one subgraph for each cluster (Gu and Zhou, 2020). Rodriguez-Sanchez et al. (2022) also proposed a multi-partition clustering that produces a set of categorical variables that encode clusters. These partitions represent a distinct clustering solution and were used as parents, leading to a more interpretable and flexible way to find clusters.

As discussed in Section 2.3, we assumed that the local distributions of phenological variables are linear mixed-effect regression models in order to allow for the partial pooling of information across clusters: this model balances the individual cluster-specific estimates with the overall trend observed in the data, leading to more stable and reliable estimates (Scutari et al., 2022). We assumed different local distributions for grain yield and the weather variables. For grain yield, we introduced a power function to model the variance after observing a skewed residual distribution during the exploratory data analysis. Moreover, we modelled grain yield with a random intercept as the only random effect; in contrast, all other phenological variables have both random coefficients and intercepts. For the weather variables, we used a linear regression model containing only fixed effects as the local distribution. We made this decision based on visual inspection, which revealed that the weather variables appeared disconnected from the clusters. This observation implies that the values of these variables were independent of both the site of origin and the variety of maize.

These assumptions reduced the prediction error for grain yield from 28% to approximately 17% when its Markov blanket or its parents were used as predictors, as shown in Figure 3. In two specific intervals, our model exhibits a higher Mean Absolute Percentage Error (MAPE) compared to the baseline model. These intervals are scenarios 7 to 11 and scenarios 19 to 24. In the first interval (7-11), our model’s performance is affected as we gradually introduce variables related to relative humidity (RH). The second interval (19-24) corresponds to the gradual inclusion of phenotypic variables. The reason for our model’s higher MAPE in these ranges could indicate that simply considering phenotypic and humidity variables is insufficient for using our model as a reliable Decision Support System (DSS). However, a notable trend emerges when we combine temperature and humidity variables (scenarios 13-18) and subsequently add phenotypic variables (24-32). During these scenarios, the MAPE of our model significantly improves compared to the baseline. Interestingly, this improvement doesn’t occur with temperature alone, where our model’s MAPE remains lower than the baseline. This suggests that the introduction of temperature as a new variable enhances the

model’s performance. This observation aligns with the causal and biological context since temperature plays a pivotal role in influencing the phenological stages of plants. Hence, incorporating temperature as a factor results in more accurate predictions. Furthermore, we assessed whether the incorporation of random effects in the structure learning procedure enhanced the local distributions, not just in terms of structure but also in terms of model specification using a backward algorithm that removes variables from the local distribution and tests the BIC, results are reported in Tables A.3 and A.4 in the appendix. Our findings indicated that random effects have a favourable impact on both structure learning and model specification. They contribute to a more accurate explanation of the data without introducing undue complexity. However, there were exceptions observed for “tassel height” and “silking”, which were best modelled without random effects. This suggests that the maxima identified with our method might be local maxima rather than global ones. Additionally, it implies that the estimation of their local distributions did not benefit from the partial pooling information provided by random effects.

Our findings confirm that a CGBN incorporating mixed-effects models to exploit the hierarchical structure of the data provides better accuracy than a standard CGBN. Considering that it is a causal model as well, we argue that it can serve as an effective decision support system, particularly in domains with inherent hierarchical structures such as the agronomic field (Burchfield et al., 2019; Li et al., 2020).

Even though our proposed method exhibits low prediction error, it comes with limitations. Firstly, the clustering pre-processing is based only on grain yield regression in order to simplify the model and to reduce the computational cost of learning it. To address this, future work will involve expanding the clustering approach to specific clusters for each phenological variable, enabling a more detailed analysis. Another limitation is the time it took to learn it: approximately 13 hours of linear time. To mitigate this, we may explore different approaches to model hierarchical data, such as the Integrated Nested Laplace Approximation (INLA; Rue et al., 2017). Moreover, in this study, we used the hill-climbing algorithm for structure learning because it compares favourably in terms of speed and structural accuracy (Scutari et al., 2019) and because our focus was on the incorporation of mixed effects. Hence, we wanted to avoid the issues with hyper-parameter tuning that are common with more complex structure learning algorithms. Other algorithms, however, may very well be more suitable for this particular type

of data and we will explore them in future work. In particular, reformulating structure learning to share information on the covariance structure of the data between iterations and variables has the potential to vastly reduce computational complexity without impacting accuracy.

5. Conclusions

Maize stands as a crucial crop for both food and feed production. Predicting its yield holds the potential to enhance farm practices and refine crop management systems. In agricultural datasets, a common hierarchical structure can be leveraged for predictive purposes, therefore, models that harness this structure tend to yield highly accurate predictions. In this study, we introduced a novel approach to learning Bayesian Networks integrating random effects into local distributions. Since the variables that encode the provenance of the field produce a dispersion of residuals in the local distribution, we made a group variable performing a hierarchical clustering based on the mean and variance of residuals from a full linear regression of maize grain yield, conditioned on the Site-variety combination. The usage of this method resulted in a reduction of prediction errors compared to the baseline model thanks to the partial pooling of information provided by the random effects. We propose its applicability as a valuable decision support system, particularly in fields marked by inherent hierarchical structures like agronomy. To enhance this tool, we could consider performing precise clustering for each phenotypical variable. Additionally, introducing alternative estimation methods, such as INLA, could reduce computational demands and empower experts to actively engage in the learning process within the Bayesian framework.

Appendix A. More details about Scenarios, Structure learning and Validation tests

Table A.1: Prediction scenarios for the grain yield of maize, identified by the set of variables used as predictors: the average temperature May-June (T1), the average temperature July-Aug (T2), the average temperature Sept-Oct (T3), the diurnal temperature range May-June (T4), the diurnal temperature range July-Aug (T5), the diurnal temperature range Sept-Oct (T6), the average RH May-June (RH1), the average RH July-Aug (RH2), the average RH Sept-Oct (RH3), the diurnal RH range May-June (RH4), the diurnal RH range July-Aug (RH5), the diurnal RH range Sept-Oct (RH6), Silking (Si), GW (Grain weight), An (Anthesis), TH (Tassel height), PH (Plant height) and EH (Ear height).

Scenario	T1	T2	T3	T4	T5	T6	RH1	RH2	RH3	RH4	RH5	RH6	Si	GW	TH	PH	An	EH
1	✓																	
2	✓	✓																
3	✓	✓		✓														
4	✓	✓		✓	✓													
5	✓	✓		✓	✓	✓												
6	✓	✓	✓	✓	✓	✓												
7							✓											
8							✓	✓										
9							✓	✓		✓								
10							✓	✓		✓	✓							
11							✓	✓		✓	✓		✓					
12							✓	✓	✓	✓	✓		✓					
13	✓						✓											
14	✓	✓					✓	✓										
15	✓	✓		✓			✓	✓		✓								
16	✓	✓		✓	✓		✓	✓		✓	✓							
17	✓	✓		✓	✓	✓	✓	✓		✓	✓							
18	✓	✓	✓	✓	✓	✓	✓	✓	✓	✓	✓							
19													✓					
20													✓	✓				
21													✓	✓	✓			
22													✓	✓	✓	✓		
23													✓	✓	✓	✓	✓	
24													✓	✓	✓	✓	✓	✓
25	✓						✓						✓					
26	✓	✓					✓	✓					✓	✓				
27	✓	✓		✓			✓	✓		✓			✓	✓	✓			
28	✓	✓		✓	✓		✓	✓		✓	✓		✓	✓	✓		✓	
29	✓	✓		✓	✓	✓	✓	✓		✓	✓		✓	✓	✓	✓	✓	
30	✓	✓	✓	✓	✓	✓	✓	✓	✓	✓	✓		✓	✓	✓	✓	✓	✓
31	✓	✓		✓	✓	✓	✓	✓	✓	✓	✓		✓	✓	✓			
32	✓	✓		✓	✓	✓	✓	✓	✓	✓	✓		✓	✓	✓			

Table A.2: New relationships found in \mathcal{B}_{LME} . Variables: the average temperature May-June (T1), the average temperature July-Aug (T2), the average temperature Sept-Oct (T3), the diurnal temperature range May-June (T4), the diurnal temperature range July-Aug (T5), the diurnal temperature range Sept-Oct (T6), the average RH May-June (RH1), the average RH July-Aug (RH2), the average RH Sept-Oct (RH3), the diurnal RH range May-June (RH4), the diurnal RH range July-Aug (RH5), the diurnal RH range Sept-Oct (RH6), Silking (Si), GW (Grain weight), An (Anthesis), TH (Tassel height), PH (Plant height) and EH (Ear height).

Parent	Child	Parent	Child
PH	→ GY	T5	→ Si
PH	→ EH	T5	→ TH
EH	→ Si	T5	→ PH
Si	→ GY	T6	→ GW
T1	→ EH	RH1	→ GY
T1	→ PH	RH2	→ GY
T2	→ An	RH3	→ GY
T2	→ TH	RH4	→ TH
T3	→ GY	RH4	→ PH
T4	→ GW	RH5	→ GY
T4	→ Si	RH5	→ EH
T4	→ TH	RH5	→ PH
T5	→ GY	RH6	→ GW

Table A.3: The BIC score values for the variables with random effects in \mathcal{B}_{LME} . The columns correspond to Silking (Si), GW (Grain weight), An (Anthesis), TH (Tassel height), PH (Plant height), EH (Ear height) and GY (Grain yield).

EH	PH	TH	An	Si	GW	GY
108448.0	128945.4	98210.88	72373.64	64279.80	127634.6	42664.90
108581.7	128988.4	131629.19	73127.37	67958.98	129620.1	42788.77
108913.9	130979.4	98721.24	72466.75	64423.46	130956.2	43600.06
109422.9	129204.0	98306.37	73802.03	78577.20	129137.0	42817.61
109076.0	128987.3	98975.48	73569.12	64617.86	128784.5	47312.45
108793.3	128996.4	99125.48	74726.54	64740.27	129580.9	42683.18
-	130634.3	98957.10	73009.51	65812.12	127641.1	44288.90
-	-	98134.49	74775.35	65272.43	129603.5	43055.93
-	-	-	75937.24	64331.62	130433.6	42733.74
-	-	-	-	64426.97	128022.4	43319.44
-	-	-	-	-	129434.5	43919.43
-	-	-	-	-	-	43890.76
-	-	-	-	-	-	44146.02
-	-	-	-	-	-	42899.58
-	-	-	-	-	-	42926.77

Table A.4: The BIC score values for the variables without random effects in \mathcal{B}_{LME} . The columns correspond to Silking (Si), GW (Grain weight), An (Anthesis), TH (Tassel height), PH (Plant height), EH (Ear height) and GY (Grain yield).

EH	PH	TH	An	Si	GW	GY
109382.7	129069.7	97997.56	72921.13	63953.28	128026.4	50158.96
109517.0	129130.9	132132.71	73968.06	67636.88	129661.0	50252.83
110087.1	131885.7	99046.89	73012.02	64104.01	131334.4	50586.06
109464.6	129540.4	98415.05	74703.04	78859.63	129263.1	50196.68
109928.2	129201.7	99377.01	74227.08	64271.16	130586.0	53345.75
109577.8	129234.8	99329.96	75441.82	64386.79	131320.9	50161.03
-	131600.8	99481.83	73857.10	65460.04	128286.2	51321.11
-	-	98304.39	75487.06	65002.78	130356.2	50378.48
-	-	-	76760.46	64166.55	132314.7	50178.26
-	-	-	-	64281.80	128579.4	50610.04
-	-	-	-	-	130592.4	51098.38
-	-	-	-	-	-	51108.30
-	-	-	-	-	-	50974.64
-	-	-	-	-	-	50306.71
-	-	-	-	-	-	50364.45

References

- Alexandratos, N., Bruinsma, J., 2012. World Agriculture: Towards 2030/2050. ESA Working Paper No. 12-03; FAO: Rome, Italy.
- Anderson, S.L., Murray, S.C., Malambo, L., Ratcliff, C., Popescu, S., Cope, D., Chang, A., Jung, J., Thomasson, J.A., 2019. Prediction of Maize Grain Yield before Maturity Using Improved Temporal Height Estimates of Unmanned Aerial Systems. *The Plant Phenome Journal* 2, 1–15. doi:10.2135/tppj2019.02.0004.
- Azzimonti, L., Corani, G., Zaffalon, M., 2019. Hierarchical Estimation of Parameters in Bayesian Networks. *Computational Statistics & Data Analysis* 137, 67–91. doi:10.1016/j.csda.2019.02.004.
- Bates, D., Mächler, M., Bolker, B., Walker, S., 2015. Fitting Linear Mixed-Effects Models using lme4. *Journal of Statistical Software* 67, 1–48. doi:10.18637/jss.v067.i01.
- Burchfield, E.K., Nelson, K.S., Spangler, K., 2019. The Impact of Agricultural Landscape Diversification on U.S. Crop Production. *Agriculture, Ecosystems & Environment* 285, 106615. doi:10.1016/j.agee.2019.106615.
- Butts-Wilmsmeyer, C.J., Seebauer, J.R., Singleton, L., Below, F.E., 2019. Weather During Key Growth Stages Explains Grain Quality and Yield of Maize. *Agronomy* 9, 16. doi:10.3390/agronomy9010016.
- Chu, T., Starek, M.J., Brewer, M.J., Murray, S.C., Pruter, L.S., 2018. Characterizing Canopy Height with UAS Structure-From-Motion Photogrammetry—Results Analysis of a Maize Field Trial with Respect to Multiple Factors. *Remote Sensing Letters* 9, 753–762. doi:10.1080/2150704X.2018.1475771.
- Coulibaly, S., Kamsu-Foguem, B., Kamissoko, D., Traore, D., 2019. Deep Neural Networks with Transfer Learning in Millet Crop Images. *Computers in Industry* 108, 115–120. doi:10.1016/j.compind.2019.02.003.
- Cussens, J., 2012. Bayesian Network Learning with Cutting Planes, in: *Proceedings of the 27th Conference on Uncertainty in Artificial Intelligence*, pp. 153–160.

- Darwiche, A., 2009. Modeling and reasoning with Bayesian networks. Cambridge University Press.
- Diebold, F., Mariano, R., 2002. Comparing Predictive Accuracy. *Journal of Business & Economic Statistics* 20, 134–144.
- Edwards, D.I., 2000. Introduction to Graphical Modelling. 2nd ed., Springer.
- FAO, IFAD, UNICEF, WFP, WHO, 2021. The State of Food Security and Nutrition in the World. URL: <https://policycommons.net/artifacts/1850109/the-state-of-food-security-and-nutrition-in-the-world-2021/2596732/>. FAO: Food and Agriculture Organization of the United Nations.
- FAOSTAT, 2019. Food Balance Sheets. URL: <http://www.fao.org/faostat/en/data/FBS>.
- Gelman, A., Carlin, J.B., Stern, H.S., Dunson, D.B., Vehtari, A., Rubin, D.B., 2014. Bayesian Data Analysis. 3rd ed., CRC Press.
- Gelman, A., Hill, J., 2007. Data Analysis Using Regression and Multi-level/Hierarchical Models. Cambridge University Press.
- Gu, J., Zhou, Q., 2020. Learning Big Gaussian Bayesian Networks: Partition, Estimation and Fusion. *The Journal of Machine Learning Research* 21, 1–31.
- Han, X., Thomasson, J.A., Bagnall, G.C., Pugh, N.A., Horne, D.W., Rooney, W.L., Jung, J., Chang, A., Malambo, L., Popescu, S.C., Gates, I.T., Cope, D.A., 2018. Measurement and Calibration of Plant-Height from Fixed-Wing UAV Images. *Sensors* 18, 4092. doi:10.3390/s18124092.
- Heckerman, D., Geiger, D., 1995. Learning Bayesian Networks: a Unification for Discrete and Gaussian Domains, in: *UAI*, pp. 274–284.
- Heisterkamp, S.H., van Willigen, E., Diderichsen, P.M., Maringwa, J., 2017. Update of the nlme Package to Allow a Fixed Standard Deviation of the Residual Error. *The R Journal* 9, 239–251. doi:10.32614/RJ-2017-010.

- Hill, E.C., Renner, K.A., Sprague, C.L., Fry, J.E., 2017. Structural Equation Modeling of Cover Crop Effects on Soil Nitrogen and Dry Bean. *Agronomy Journal* 109, 2781–2788. doi:10.2134/agronj2016.12.0712.
- Ilić, M., Mutavdžić, B., Srdević, Z., Srdević, B., 2022. Irrigation Water Fitness Assessment Based on Bayesian Network and FAO Guidelines. *Irrigation and Drainage* 71, 665–675. doi:10.1002/ird.2676.
- Koller, D., Friedman, N., 2009. Probabilistic Graphical Models: Principles and Techniques. MIT Press.
- Krishna, M.V., Swaroopa, K., SwarnaLatha, G., YasaSwani, V., 2023. Crop Yield Prediction in India Based on Mayfly Optimization Empowered Attention-Bi-Directional Long Short-Term Memory (LSTM). *Multimedia Tools and Applications* Online first, 1–28. doi:10.1007/s11042-023-16807-7.
- Leroux, L., Castets, M., Baron, C., Escorihuela, M.J., Bégué, A., Lo Seen, D., 2019. Maize Yield Estimation in West Africa from Crop Process-Induced Combinations of Multi-Domain Remote Sensing Indices. *European Journal of Agronomy* 108, 11–26. doi:10.1016/j.eja.2019.04.007.
- Li, Z., Taylor, J., Yang, H., Casa, R., Jin, X., Li, Z., Song, X., Yang, G., 2020. A Hierarchical Interannual Wheat Yield and Grain Protein Prediction Model Using Spectral Vegetative Indices and Meteorological Data. *Field Crops Research* 248, 107711. doi:10.1016/j.fcr.2019.107711.
- Lu, W., Newlands, N.K., Carisse, O., Atkinson, D.E., Cannon, A.J., 2020. Disease Risk Forecasting with Bayesian Learning Networks: Application to Grape Powdery Mildew (*Erysiphe necator*) in Vineyards. *Agronomy* 10, 622. doi:10.3390/agronomy10050622.
- Malik, H.N., Malik, S.I., Hussain, M., Chughtai, S.U.R., Javed, H.I., 2005. Genetic Correlation among Various Quantitative Characters in Maize (*Zea mays* L.) Hybrids. *Journal of Agriculture & Social Sciences* 1, 262–265.
- Millet, E., Welcker, C., Kruijjer, W., Negro, S., Nicolas, S., Praud, S., Ranc, N., Presterl, T., Tuberosa, R., Bedo, Z., Draye, X., Usadel, B., Charcosset, A., van Eeuwijk, F., Tardieu, F., Coupel-Ledru, A., Bauland, C., 2016. Genome-Wide Analysis of Yield in Europe: Allelic Effects as Functions

- of Drought and Heat Scenarios. *Plant Physiology* 172, 749–764. doi:10.1104/pp.16.00621.
- Millet, E.J., Pommier, C., Buy, M., Nagel, A., Kruijer, W., Welz-Bolduan, T., Lopez, J., Richard, C., Racz, F., Tanzi, F., Spitkot, T., Canè, M.A., Negro, S.S., Coupel-Ledru, A., Nicolas, S.D., Palaffre, C., Bauland, C., Praud, S., Ranc, N., Presterl, T., Bedo, Z., Tuberosa, R., Usadel, B., Charcosset, A., van Eeuwijk, F., Draye, X., Tardieu, F., Welcker, C., 2019. A Multi-Site Experiment in a Network of European Fields for Assessing the Maize Yield Response to Environmental Scenarios. doi:10.15454/IASSTN.
- Mupangwa, W., Chipindu, L., Nyagumbo, I., Mkuhlani, S., Sisito, G., 2020. Evaluating Machine Learning Algorithms for Predicting Maize Yield Under Conservation Agriculture in Eastern and Southern Africa. *SN Applied Sciences* 2, 952. doi:10.1007/s42452-020-2711-6.
- Murtagh, F., Legendre, P., 2014. Ward’s Hierarchical Agglomerative Clustering Method: Which Algorithms Implement Ward’s Criterion? *Journal of Classification* 31, 274–295. doi:10.1007/s00357-014-9161-z.
- Ndlovu, N., Spillane, C., McKeown, P.C., Cairns, J.E., Das, B., Gowda, M., 2022. Genome-Wide Association Studies of Grain Yield and Quality Traits under Optimum and Low-Nitrogen Stress in Tropical Maize (*Zea mays* L.). *Theoretical and Applied Genetics* 135, 4351–4370. doi:10.1007/s00122-022-04224-7.
- Neiff, N., Trachsel, S., Valentinuz, O.R., Balbi, C.N., Andrade, F.H., 2016. High Temperatures around Flowering in Maize: Effects on Photosynthesis and Grain Yield in Three Genotypes. *Crop Science* 56, 2702–2712. doi:10.2135/cropsci2015.12.0755.
- Oyen, D., Lane, T., 2015. Transfer Learning for Bayesian Discovery of Multiple Bayesian Networks. *Knowledge and Information Systems* 43, 1–28. doi:10.1007/s10115-014-0775-6.
- Pan, S.J., Yang, Q., 2010. A Survey on Transfer Learning. *IEEE Transactions on Knowledge and Data Engineering* 22, 1345–1359. doi:10.1109/TKDE.2009.191.
- Patterson, H.D., Williams, E.R., 1976. A New Class of Resolvable Incomplete Block Designs. *Biometrika* 63, 83–92. doi:10.1093/biomet/63.1.83.

- Paymode, A.S., Malode, V.B., 2022. Transfer Learning for Multi-Crop Leaf Disease Image Classification using Convolutional Neural Network VGG. *Artificial Intelligence in Agriculture* 6, 23–33. doi:10.1016/j.aiia.2021.12.002.
- Pearl, J., 2009. *Causality: Models, Reasoning and Inference*. 2nd ed., Cambridge University Press.
- Pettet, G., Nannapaneni, S., Stadnick, B., Dubey, A., Biswas, G., 2017. Incident Analysis and Prediction Using Clustering and Bayesian Network, in: 2017 IEEE SmartWorld, Ubiquitous Intelligence & Computing, Advanced & Trusted Computed, Scalable Computing & Communications, Cloud & Big Data Computing, Internet of People and Smart City Innovation (SmartWorld/SCALCOM/UIC/ATC/CBDCOM/IOP/SCI), pp. 1–8. doi:10.1109/UIC-ATC.2017.8397587.
- Pew Research Center, 2019. World’s Population is Projected to Nearly Stop Growing by the End of the Century. URL: <https://www.pewresearch.org/short-reads/2019/06/17/>.
- Pinheiro, J.C., Bates, D.M., 2000. *Mixed-Effects Models in S and S-PLUS*. Springer.
- Pugh, N.A., Horne, D.W., Murray, S.C., Carvalho Jr, G., Malambo, L., Jung, J., Chang, A., Maeda, M., Popescu, S., Chu, T., Starek, M.J., Brewer, M.J., Richardson, G., Rooney, W.L., 2018. Temporal Estimates of Crop Growth in Sorghum and Maize Breeding Enabled by Unmanned Aerial Systems. *The Plant Phenome Journal* 1, 1–10. doi:10.2135/tppj2017.08.0006.
- Qian, S.S., Cuffney, T.F., Alameddine, I., McMahon, G., Reckhow, K.H., 2010. On the application of multilevel modeling in environmental and ecological studies. *Ecology* 91, 355–361. doi:10.1890/09-1043.1.
- Rodriguez-Sanchez, F., Bielza, C., Larrañaga, P., 2022. Multipartition Clustering of Mixed Data with Bayesian Networks. *International Journal of Intelligent Systems* 37, 2188–2218. doi:10.1002/int.22770.
- Rotili, D.H., de Voil, P., Eyre, J., Serafin, L., Aisthorpe, D., Maddonni, G.A., Rodríguez, D., 2020. Untangling Genotype x Management Interactions in

- Multi-Environment On-Farm Experimentation. *Field Crops Research* 255, 107900. doi:10.1016/j.fcr.2020.107900.
- Rue, H., Riebler, A., Sørbye, S.H., Illian, J.B., Simpson, D.P., Lindgren, F.K., 2017. Bayesian Computing with INLA: A Review. *Annual Review of Statistics and Its Application* 4, 395–421. doi:10.1146/annurev-statistics-060116-054045.
- Russell, S.J., Norvig, P., 2009. *Artificial Intelligence: A Modern Approach*. 3rd ed., Prentice Hall.
- Schwarz, G., 1978. Estimating the Dimension of a Model. *The Annals of Statistics* 6, 461–464.
- Scutari, M., 2010. Learning Bayesian Networks with the bnlearn R Package. *Journal of Statistical Software* 35, 1–22.
- Scutari, M., Graafland, C.E., Gutiérrez, J.M., 2019. Who Learns Better Bayesian Network Structures: Accuracy and Speed of Structure Learning Algorithms. *International Journal of Approximate Reasoning* 115, 235–253.
- Scutari, M., Marquis, C., Azzimonti, L., 2022. Using Mixed-Effects Models to Learn Bayesian Networks from Related Data Sets. *Proceedings of Machine Learning Research* 186, 73–84.
- Spiegelhalter, D.J., Abrams, K.R., Myles, J.P., 2004. *Bayesian Approaches to Clinical Trials and Health-Care Evaluation*. Wiley.
- Spirtes, P., Glymour, C., Scheines, R., 2000. *Causation, Prediction, and Search*. MIT Press.
- Tolley, S.A., Brito, L.F., Wang, D.R., Tuinstra, M.R., 2023. Genomic Prediction and Association Mapping of Maize Grain Yield in Multi-Environment Trials Based on Reaction Norm Models. *Frontiers in Genetics* 14, 1221751.
- Waqas, M.A., Wang, X., Zafar, S.A., Noor, M.A., Hussain, H.A., Azher Nawaz, M., Farooq, M., 2021. Thermal Stresses in Maize: Effects and Management Strategies. *Plants* 10, 293. doi:10.3390/plants10020293.

- Yan, H., Song, S., Wang, F., He, D., Zhao, J., 2023. Operational Adjustment Modeling Approach Based on Bayesian Network Transfer Learning for New Flotation Process Under Scarce Data. *Journal of Process Control* 128, 103000. doi:10.1016/j.jprocont.2023.103000.
- Yang, B., Zhu, W., Rezaei, E.E., Li, J., Sun, Z., Zhang, J., 2022. The Optimal Phenological Phase of Maize for Yield Prediction with High-Frequency UAV Remote Sensing. *Remote Sensing* 14, 1559. doi:10.3390/rs14071559.
- Yang, W., Nigon, T., Hao, Z., Dias Paiao, G., Fernández, F.G., Mulla, D., Yang, C., 2021. Estimation of Corn Yield Based on Hyperspectral Imagery and Convolutional Neural Network. *Computers and Electronics in Agriculture* 184, 106092. doi:10.1016/j.compag.2021.106092.
- Yin, X., McClure, M.A., Jaja, N., Tyler, D.D., Hayes, R.M., 2011. In-Season Prediction of Corn Yield Using Plant Height under Major Production Systems. *Agronomy Journal* 103, 923–929. doi:10.2134/agronj2010.0450.
- Zhang, L., Zhang, Z., Luo, Y., Cao, J., Xie, R., Li, S., 2021. Integrating Satellite-Derived Climatic and Vegetation Indices to Predict Smallholder Maize Yield Using Deep Learning. *Agricultural and Forest Meteorology* 311, 108666. doi:10.1016/j.agrformet.2021.108666.
- Zorić, M., Gunjača, J., Galić, V., Jukić, G., Varnica, I., Šimić, D., 2022. Best Linear Unbiased Predictions of Environmental Effects on Grain Yield in Maize Variety Trials of Different Maturity Groups. *Agronomy* 12, 922. doi:10.3390/agronomy12040922.